

Comparing the Space Densities of Millisecond-Spin Magnetars and Fast X-Ray Transients

S. Biswas^{1*}, P. G. Jonker^{1,2}, M. Coleman Miller³, A. Levan^{1,4}, J. Quirola-Vásquez¹

¹ Department of Astrophysics/IMAPP, Radboud University, PO Box 9010, 6500 GL, The Netherlands

² SRON, Netherlands Institute for Space Research, Niels Bohrweg 4, Leiden, 2333 CA, The Netherlands

³ Department of Astronomy and Joint Space-Science Institute, University of Maryland, College Park, 20742, Maryland, USA

⁴ Department of Physics, University of Warwick, Coventry, CV4 7AL, UK

Received XXX; accepted YYY

ABSTRACT

Context. Fast X-Ray Transients (FXTs) are bright X-ray flashes with durations of a few minutes to hours, peak isotropic luminosities of $L_{X,\text{peak}} \sim 10^{42} - 10^{47} \text{ erg s}^{-1}$, and total isotropic energies of $E \sim 10^{47} - 10^{50} \text{ erg}$, which have been detected with space-based telescopes such as *Chandra*, *XMM-Newton*, *Swift-XRT*, and *Einstein Probe* in the soft X-ray band. *Einstein Probe* has detected >50 in its first year of operation. While several models have been proposed, the nature of many FXTs is currently unknown. One model predicts that FXTs are powered by the spin-down energy of newly-formed millisecond magnetars. In this context, they are usually thought to form in a binary neutron star (BNS) merger. However, the rates seem to be in tension: the BNS volumetric rate is estimated to be $\sim 10^2 \text{ Gpc}^{-3} \text{ yr}^{-1}$, which barely overlaps with the estimated FXT volumetric rate of $10^3 - 10^4 \text{ Gpc}^{-3} \text{ yr}^{-1}$, and thus even in the small range of overlap BNS mergers would need to produce FXTs with nearly 100% efficiency.

Aims. We explore the maximum volumetric formation rate of millisecond spin period magnetars, including several possibilities beyond the BNS channel, comparing it with the volumetric rate of FXTs, to determine what fraction of FXTs could arise from a millisecond magnetar origin.

Methods. We compile the estimated rate densities for several different suggested formation channels of rapidly spinning magnetars, including the accretion-induced collapse of white dwarfs, binary white dwarf mergers, neutron star – white dwarf mergers, and the collapse of massive stars. We convert the Milky Way event rates to volumetric rates, wherever necessary, by considering either the star formation rate or the stellar mass density distributions as a function of redshift.

Results. We find that the highest possible rates among these possibilities come from binary white dwarf mergers and the collapse of massive stars. However, both scenarios may be unfavourable for FXT production, due to uncertainties in the resultant spin and magnetic field distributions of the newly formed neutron stars, and several observational constraints. Moreover, in all the scenarios, we find that the fraction of neutron stars that meet both criteria of rapid rotation and a strong magnetic field strength is either very low or highly uncertain. We conclude that millisecond magnetars are not the most viable progenitors of FXTs, and can account for at most 10% of the entire FXT population.

Key words. X-ray: bursts - Stars: evolution - Stars: magnetars

1. Introduction

Fast X-ray transients (FXTs) are short X-ray flashes with durations of a few minutes to hours, which have been observed in the $\sim 0.3\text{--}10 \text{ keV}$ X-ray band by *Chandra*, *XMM-Newton*, *Swift-XRT* and *Einstein Probe* (e.g., Soderberg et al. 2008; Jonker et al. 2013; Glennie et al. 2015; Irwin et al. 2016; Bauer et al. 2017; Lin et al. 2018; Xue et al. 2019; Alp & Larsson 2020; Novara et al. 2020; Lin et al. 2020; Ide et al. 2020; Pastor-Marazuela et al. 2020; Wilms et al. 2020; Lin et al. 2021, 2022; Eppachen et al. 2023; Quirola-Vásquez et al. 2022, 2023; Levan et al. 2024a; Gillanders et al. 2024; Liu et al. 2024). They are characterized by a single highly energetic outburst, with peak isotropic luminosities of $L_{X,\text{peak}} \sim 10^{42} - 10^{47} \text{ erg s}^{-1}$. So far, ~ 30 extragalactic FXTs have been identified through careful archival searches. The first FXT detected with contemporaneous multi-wavelength observations was XRT 080109/SN 2008D,

which was serendipitously observed by *Swift* during a supernova observation (Soderberg et al. 2008; Mazzali et al. 2008; Modjaz et al. 2009).

In early 2024, *Einstein Probe* (EP) was launched (Yuan et al. 2015, 2022), and it has announced the discovery of several FXTs in near real-time (e.g., Pan et al. 2024a; Zhang et al. 2024; Wu(NAOC et al. 2024; Pan et al. 2024b; Zhou et al. 2024; Sun et al. 2024). This has led to prompt multi-wavelength follow-up observations of FXTs, helping us understand their origin. For example, Zhang et al. (2024) reported EP 240315a and it led to the first detection of both an optical and radio counterpart of an EP-discovered FXT, detected at a redshift of $z = 4.859$ (Gillanders et al. 2024; Srivastav et al. 2024; Saccardi et al. 2024; Carotenuto et al. 2024; Bruni et al. 2024; Leung et al. 2024; Levan et al. 2024a). Levan et al. (2024a) concluded that the observed properties of EP 240315a are potentially consistent with a long GRB (collapsar) interpretation of FXTs (also see Gillanders et al. 2024 and Liu et al. 2024).

* e-mail: sumedha.biswas@ru.nl

While the origin of the majority of FXTs is unknown, several theories have been put forward: (1) X-ray emission produced during the spindown of a millisecond magnetar produced in a binary neutron star (BNS) merger (e.g., Dai et al. 2018; Fong et al. 2015; Sun et al. 2017; Bauer et al. 2017; Xue et al. 2019); (2) supernova shock breakouts (SBO) from core-collapse supernovae (CCSNe), where the X-ray emission is generated from the breakout of the supernova explosion once it crosses the surface of an evolved star such as a blue supergiant or a Wolf-Rayet star (e.g., Soderberg et al. 2008; Nakar & Sari 2010; Waxman & Katz 2017; Novara et al. 2020; Alp & Larsson 2020); (3) tidal disruption event (TDE) involving a white dwarf (WD) and intermediate mass black hole (IMBH), where X-rays are produced by the accretion disc and/or relativistic jet (e.g., Jonker et al. 2013; MacLeod et al. 2014; Saxton et al. 2021; Maguire et al. 2020); (4) X-ray emission from off-axis or sub-luminous gamma-ray bursts (GRBs), produced by the mildly relativistic cocoon jet once it breaks the surface of a massive progenitor star (e.g., Ramirez-Ruiz et al. 2002; Zhang et al. 2004; Nakar 2015; Zhang et al. 2018; D'Elia et al. 2018). Several of these theories have been probed by studying the host galaxies of some FXTs, and the offset of the FXT with respect to the centre of the host, where a larger offset potentially implies an older system (e.g., Eappachen et al. 2022, 2023, 2024; Inkenhaag et al. 2024; Quirola-Vázquez et al. 2025).

In this work, we investigate the millisecond magnetar model for FXTs. The ultimate source of energy for millisecond magnetar-powered FXTs is rotational, with $E_{\text{rot}} \approx 2 \times 10^{52} \text{ erg } (I/10^{45} \text{ g cm}^2)(\nu/1000 \text{ Hz})^2$, where I and ν are the moment of inertia and the spin frequency of the neutron star, respectively. Thus, there is in principle plenty of rotational energy in the millisecond magnetars to explain FXTs. If the duration of an FXT is similar to its magnetic dipole spindown time, then a $B \sim 10^{14} - 10^{16} \text{ G}$ with a birth frequency $\nu = 1000 \text{ Hz}$ would be consistent with the typically observed duration of a few minutes to a few hours for individual FXTs and luminosities of $L_{X,\text{peak}} \sim 10^{42} - 10^{47} \text{ erg s}^{-1}$, assuming that the efficiency η of X-ray production is of the order of $\sim 10^{-3} - 10^{-2}$ (η is defined as L_X/L_{sd} , where L_X is the X-ray luminosity and L_{sd} is the spin-down luminosity).

If millisecond magnetars originate from binary neutron star (BNS) mergers, then a positive feature of this model is that these mergers typically expel only $\sim 10^{-4} - 10^{-2} M_{\odot}$ (e.g., Hotokezaka et al. 2013) of material. While this ejecta contains significant amounts of r-process elements with high opacity, its rapid expansion leads to decreasing density over time, potentially allowing X-ray radiation to escape as the ejecta becomes optically thin. Previous studies have modelled and calculated the optical/UV and X-ray emission expected from the spindown of millisecond magnetars produced from BNS mergers, and predicted their light curves (e.g., Zhang 2013; Siegel & Ciolfi 2016; Siegel & Ciolfi 2016; Sun et al. 2017). Two FXTs were identified in the 7 Ms *Chandra* Deep Field-South (CDF-S) data set, XRT 141001 (Bauer et al. 2017) and XRT 150322 (Zheng et al. 2017), denoted also as "CDS-XT1" and "CDS-XT2", respectively. Motivated by the above spin-down magnetar models, Sun et al. (2019) (see their figure 2) interpret both CDS-XT1 and CDS-XT2 within the framework of the BNS merger millisecond magnetar model.

However, the rate of BNS mergers is in tension with the rate of FXTs. The volumetric rate of known distant extragalactic FXTs is $\sim 10^3 - 10^4 \text{ Gpc}^{-3} \text{ yr}^{-1}$ (Quirola-Vázquez et al. 2022, 2023). In comparison, the volumetric rate of BNS mergers is $\sim 10^1 - 10^3 \text{ Gpc}^{-3} \text{ yr}^{-1}$ from GW detections through LVK run O3 (e.g., Mandel & Broekgaarden 2022; Abbott et al. 2023). Although the upper limit of the BNS merger rate overlaps with the lower limit of the FXT rate, it would require an efficiency close to unity to account for all FXTs, i.e., assuming that each BNS merger results in an FXT. Depending on the neutron star equation of state, the masses of the two neutron stars before merger, and their mass ratio, the merger product could however, also be a black hole (Metzger 2019).

Here we therefore also consider the formation of millisecond magnetars through other channels such as the accretion-induced collapse (AIC) of white dwarfs (e.g., Miyaji et al. 1980), binary white dwarf (BWD) mergers (e.g., Levan et al. 2006), neutron star - white dwarf (NSWD) mergers (e.g., Metzger 2012), and the collapse of massive stars (e.g., Beniamini et al. 2019).

In Section 2, we review the formation scenarios of rapidly spinning magnetars. In Section 3, we discuss the combined rate of formation of magnetars (Table 2), and we discuss other constraints such as the uncertainties in the spin distributions, the effects of the surrounding post-merger ejecta, the duration of FXTs, and the consequent implications for their origin. Wherever relevant, we have converted the event rates to volumetric rates using one of the two methods described in Appendix 3.1. We conclude in Section 4.

2. Rate of Formation of Rapidly Spinning Magnetars

In the following sections, we describe the various formation pathways for rapidly spinning magnetars as summarized in Figure 1.

2.1. Pathway A: Binary White Dwarfs

The Milky Way (MW) contains $\sim 10^{10}$ WDs, of which about $(2 - 3) \times 10^8$ are thought to exist in binaries with other WDs (Nelemans et al. 2001; Holberg 2009; Napiwotzki 2009). About half of these binaries are predicted to merge within a Hubble time. The BWD merger rate has been estimated by, for example, Nelemans et al. (2001) to be $3 \times 10^{-3} \text{ yr}^{-1}$ in the MW for binaries with total masses higher than M_{Ch} , where $M_{\text{Ch}} \approx 1.4 M_{\odot}$ is the Chandrasekhar mass (Chandrasekhar 1931).

The final outcome of a BWD merger, whether it produces a magnetar or not, depends on the properties of the WDs involved. Different combinations of WD binaries, for example, CO+CO, CO+ONe, and ONe+ONe¹ lead to different merger remnants (e.g., Dan et al. 2013; Liu & Wang 2020). However, their outcomes are not well understood yet. Here, we consider CO+CO WD binaries, which account for $\sim 25\%$ of all BWDs in the MW (Nelemans et al. 2001), although some recent studies also suggest other types of WD mergers such as ONe+CO WD binaries as progenitors for NSs (and potentially magnetars) (e.g., Kashyap et al. 2018;

¹ CO: Carbon-Oxygen; ONe: Oxygen-Neon;

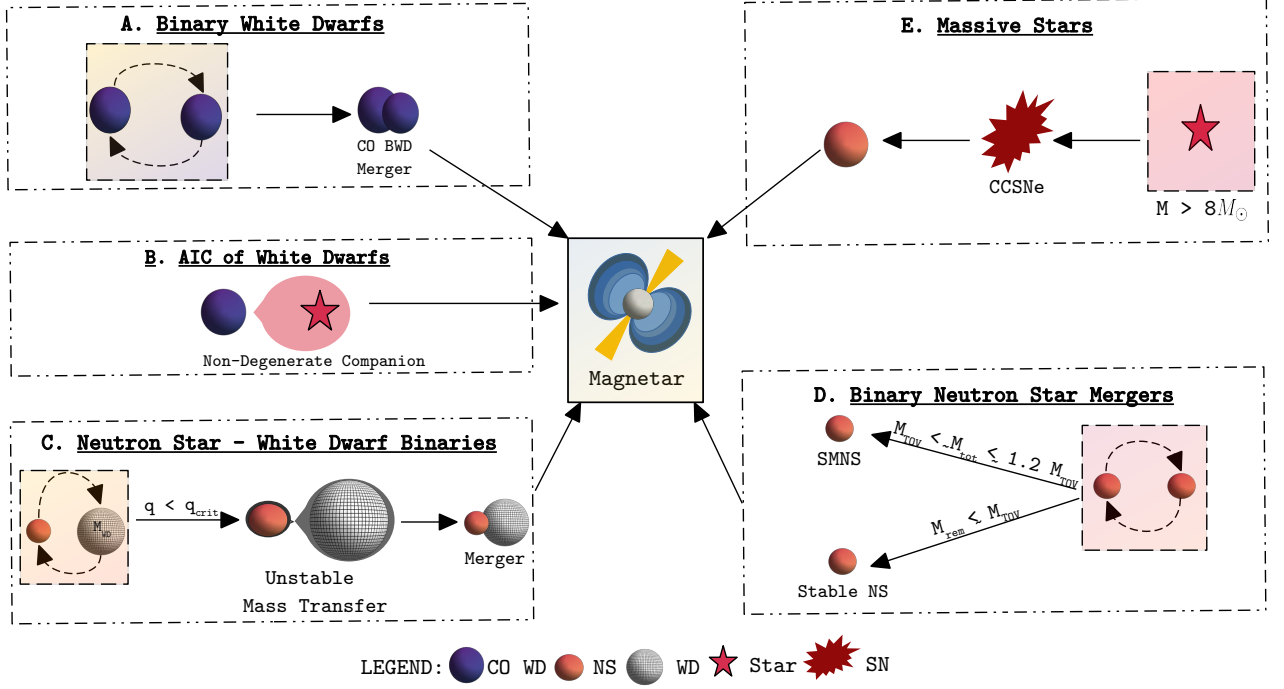


Fig. 1. Schematic diagram to summarize the different formation mechanisms of rapidly spinning magnetars: (A) Binary white dwarf mergers (B) Accretion-induced collapse of massive white dwarfs (C) Neutron star-white dwarf mergers (D) Binary neutron star mergers (E) Collapse of massive stars

Wu et al. 2023). We consider two CO WDs in a binary, with a total binary mass of $M = M_{WD1} + M_{WD2}$, where M_{WD1} and M_{WD2} are the individual masses of the WDs that eventually merge.

If $M > M_{Ch}$, the CO WD merger would typically result in the explosion of the more massive WD (e.g., Hachisu et al. 1996; Li & van den Heuvel 1997; Wang et al. 2009; Shen et al. 2012; Wang et al. 2013; Wu et al. 2016; Wang 2018; Perets et al. 2019), resulting in a Type Ia supernova (SN). However, if one or both WDs have very strong magnetic field strengths ($\gtrsim 2 \times 10^6$ G), it could produce a rapidly spinning magnetar after the merger (King et al. 2001; Levan et al. 2006), alternatively, angular momentum may be transferred from the center to the outer regions, enabling the formation of a disk around the newly formed compact object (e.g., Külebi et al. 2013). About 10% of the WD population has sufficiently strong magnetic field strengths, which implies an upper limit for the rate of formation of a msec. spin magnetar as $3 \times 10^{-4} \text{ yr}^{-1}$ in the MW (Levan et al. 2006).

2.2. Pathway B: Accretion-Induced Collapse of Massive White Dwarfs

Another scenario for the formation of a NS (and potentially a millisecond magnetar) is the accretion-induced collapse (AIC) of a massive WD, after it accretes matter from a non-degenerate companion such as a main-sequence star, a red giant, or a He star (e.g., Tauris et al. 2013; Schwab et al. 2016), and its mass increases. If $M > M_{Ch}$, the massive WDs are predicted to collapse into NSs due to the rapid electron-captures onto heavy elements produced by

the oxygen burning, preventing a thermonuclear explosion (e.g., Miyaji et al. 1980). NS formation is considered to be the most likely outcome of AIC of a WD, however, also see Jones et al. (2016, 2019) for discussions about alternative scenarios where a thermonuclear explosion occurs. The produced NS has millisecond spins due to the conservation of angular momentum; as the WD collapses, its radius decreases, causing its rotation rate to increase significantly (Duncan & Thompson 1992; Price & Rosswog 2006; Zrake & MacFadyen 2013). Additionally, the rapid rotation, combined with the dynamics of the collapse, may lead to the amplification of any pre-existing magnetic fields and the generation of strong magnetic fields, resulting in surface dipole fields on the order of $10^{14} - 10^{15}$ G, characteristic of magnetars (Piro & Kollmeier 2016). Yungelson & Livio (1998) determined the AIC event rate in the MW to be $8 \times 10^{-7} - 8 \times 10^{-5} \text{ yr}^{-1}$, and Piro & Kollmeier (2016) further estimated that a fraction of 0.01 – 0.1 of AIC of massive WD events produce a millisecond magnetar, corresponding to $\sim 10^{-9} - 10^{-6} \text{ yr}^{-1}$.

2.3. Pathway C: Neutron Star-White Dwarf Binaries

A standard scenario for the formation of a tight NS-WD binary invokes common envelope evolution of an initially wide binary, consisting of a NS and an intermediate-mass ($\lesssim 8 - 10 M_{\odot}$) main-sequence companion (e.g. van den Heuvel & Bonsema 1984) which eventually forms a WD. The composition of the WD has a high probability of being CO, but it could also be ONe, Helium (He) or He-CO (Toonen et al. 2018). Eventually, a tight NS-WD binary is formed, and the system continues to lose orbital angular momen-

tum on long timescales due to gravitational wave emission (see Peters 1964 for inspiral time calculations).

The outcome of the merger of two compact objects with masses M_{WD} and M_{NS} in a NS-WD binary is dependent upon the critical mass ratio $q_{\text{crit}} = M_{\text{WD,crit}}/M_{\text{NS}}$, where $M_{\text{WD,crit}}$ is the critical WD mass. Bobrick et al. (2017) established $M_{\text{WD,crit}} = 0.2 M_{\odot}$, a value lower than previous estimates but considered to be more robust due to its incorporation of efficient angular momentum loss through disc winds. Toonen et al. (2018) suggested that over 99.9% of semidetached NS-WD binaries would merge when $M_{\text{WD,crit}} = 0.2 M_{\odot}$. There are $\gtrsim 20$ NS-WD binaries identified in the MW (Lorimer 2005), of which 4 are predicted to merge in $\lesssim 10^{10}$ years (see Metzger 2012 for references). Close NS-WD binaries can also be formed directly by collisions in dense stellar regions, such as the centres of galaxies or globular clusters (Sigurdsson & Rees 1997).

Based on the observed properties of the NS-WD binaries in our MW (such as their masses and orbital periods), Kim et al. (2004) estimated a merger rate of $10^{-6} - 10^{-5} \text{ yr}^{-1}$ in the MW. Some population synthesis models predict higher rates of $10^{-5} - 10^{-3} \text{ yr}^{-1}$ in the MW (e.g., Portegies Zwart & Yungelson 1999; Tauris & Sennels 2000; Davies et al. 2002). Thompson et al. (2009) estimated the volumetric event rate of NS-WD mergers in the local universe to be $(0.5 - 1) \times 10^4 \text{ Gpc}^{-3} \text{ yr}^{-1}$.

If $q < q_{\text{crit}}$, unstable mass transfer takes place as the WD is tidally disrupted by the NS on dynamical timescales, leading to a merger (e.g., Hjellming & Webbink 1987). Margalit & Metzger (2016) suggested that a NS-WD merger would lead to the formation of a millisecond pulsar surrounded by an accretion disk. The magnetic field strength of the NS may either increase via a dynamo winding-up process (Paschalidis et al. 2011) or decrease through enhanced ohmic dissipation of accreted matter in the crust of the NS (Konar & Bhattacharya 1997; Urpin et al. 1997; Cumming et al. 2004). Zhong & Dai (2020) found that during the unstable mass transfer process, the magnetic field of the NS undergoes amplification via an $\alpha - \omega$ dynamo mechanism. This occurs as the accreting NS becomes enveloped by a massive, extended hot disk composed of WD debris, potentially resulting in the formation of a millisecond magnetar. It is difficult to ascertain the exact fraction of magnetars formed from this NS-WD merger pathway. If we follow the assumption made in Zhong & Dai (2020) that the magnetar formation rate through this channel is similar to the BNS merger rate i.e., 3% of all NS-WD mergers (Nicholl et al. 2017), then the volumetric rate is $150 - 300 \text{ Gpc}^{-3} \text{ yr}^{-1}$. However, as there is no clear justification given for this assumption, and as this scenario requires further numerical/observational studies, we note that the millisecond magnetar formation rate through this channel is highly uncertain.

2.4. Pathway D: Binary Neutron Stars

The merger of two NSs has four possible outcomes (see table 3 in Metzger 2019 for mass ranges, lifetimes and rates of each outcome) that for instance, depend on the total mass of the binary, M_{tot} (Shibata & Uryū 2000; Shibata & Taniguchi 2006), and the nuclear equation-of-state (EoS) which sets the maximum allowed non-rotating NS mass, M_{TOV} . For example, Margalit & Metzger (2017) determine

$M_{\text{TOV}} \lesssim 2.7 M_{\odot}$ (see their figure 4 and table 2 for details about the dependence on the EoS).

If $M_{\text{rem}} \lesssim M_{\text{TOV}}$, the merger results in a stable NS that can live indefinitely. For $M_{\text{TOV}} \lesssim M_{\text{tot}} \lesssim 1.2 M_{\text{TOV}}$, a supramassive NS (SMNS) is produced, which remains stable for $\gg 300$ ms before collapsing to a black hole (BH). When $M_{\text{crit}} \gtrsim M_{\text{tot}} \gtrsim M_{\text{TOV}}$, a hypermassive NS (HMNS) forms with strong differential rotation and typically collapses into a BH within seconds to minutes (Metzger 2019). If $M_{\text{tot}} > M_{\text{crit}}$, where $M_{\text{crit}} \sim 2.6 - 3.9 M_{\odot}$ (Hotokezaka et al. 2011; Bauswein et al. 2013), the remnant collapses to form a BH almost immediately after merger. If the remnant NS survives the merger, it is expected to have a millisecond spin period due to conservation of orbital angular momentum during the inspiral and merger phases (e.g., Shibata & Uryū 2000; Hotokezaka et al. 2011). Furthermore, during the merger, shear flows and turbulence driven by the Kelvin-Helmholtz instability enhance magnetic field strengths ($B \sim 10^{14} - 10^{16} \text{ G}$) through small-scale dynamo mechanisms (e.g., Giacomazzo et al. 2015).

However, remnant stability is not guaranteed by the condition of $M < 1.2 M_{\text{TOV}}$ alone; Beniamini & Lu (2021) show that SMNSs collapse into a BH after shedding $\sim (3 - 6) \times 10^{52} \text{ erg}$ of rotational energy before collapsing into a BH, with survival timescales sensitive to their magnetic field strength and angular momentum transport efficiency. Furthermore, Margalit et al. (2022) demonstrate that the angular momentum profile of the SMNS influences its stability: differential rotation provides temporary centrifugal support, but magnetorotational instabilities (MRI) redistribute angular momentum in regions of decreasing angular velocity, while solid-body rotation in the core enhances stability. These effects imply that only a fraction of SMNS remnants ($M_{\text{tot}} < 1.2 M_{\text{TOV}}$) avoid rapid collapse, depending on the energy loss and angular momentum redistribution timescales.

The discovery of NSs with masses $\sim 2 M_{\odot}$ (Demorest et al. 2010; Antoniadis et al. 2013; Romani et al. 2022) establishes a lower limit on M_{TOV} , while the upper limit of $\sim 2.1 - 2.2 M_{\odot}$ can be inferred from the detection of GW170817 and the corresponding EM counterpart detections; these estimates depend on assumptions such as the EoS (e.g., Margalit & Metzger 2017; Granot et al. 2017; Shibata et al. 2017; Shao et al. 2020). While BNS mergers with total mass $M_{\text{tot}} > M_{\text{crit}}$ result in prompt BH formation, the existence of massive NSs implies that some merger remnants must have masses $< M_{\text{crit}}$, allowing for the formation of millisecond magnetars rather than promptly collapsing into BHs.

The rate of formation of millisecond magnetars could potentially be constrained observationally in several ways, assuming current theoretical models of kilonovae are accurate. First, a millisecond magnetar central engine is predicted to release more energy than is observed in SGRBs, as indicated by early-time X-ray and gamma-ray detections—such as the absence of extended emission or internal plateaus, and late-time radio follow-up observations (Horesh et al. 2016; Schroeder et al. 2020; Beniamini & Lu 2021; Ricci et al. 2021). Secondly, such mergers are predicted to produce kilonovae that are significantly brighter than those without a millisecond magnetar remnant, which are inconsistent with limits from all-sky optical surveys such as ZTF (Wang et al. 2023). Lastly, these mergers are expected to produce kilonova afterglows that are brighter

and peak earlier than those without a millisecond magnetar remnant, but no such afterglows have been observed till date (Acharya et al. 2025). Additionally, the rate of BNS mergers from GW observations is $\sim 10^1 - 10^3 \text{ Gpc}^{-3} \text{ yr}^{-1}$ (e.g. Mandel & Broekgaarden 2022; Abbott et al. 2023), which provides an upper limit for the rate of formation of millisecond magnetars from this channel.

2.5. Pathway E: Massive Stars

Massive stars ($\gtrsim 8 M_\odot$) end their lives with a core-collapse supernova (CCSN), leaving behind a compact object (NS or BH), at a rate of $10^5 - 10^6 \text{ Gpc}^{-3} \text{ yr}^{-1}$ (Eldridge et al. 2019), the majority of these systems are likely to form NSs. It is likely that the majority of the ~ 30 magnetars observed within the MW (Olausen & Kaspi 2014) arise via this channel given their locations in the Galactic plane, associations with star-forming regions (e.g., Tendulkar et al. 2012), and in some cases, direct locations at the centre of SNe remnants (Lyman et al. 2022). Recent estimates suggest that a substantial fraction of neutron stars, $0.4^{+0.6}_{-0.28}$, may be born as magnetars (Beniamini et al. 2019). This is consistent with previous studies that proposed approximately 10% of CC-SNe form magnetars (Kouveliotou et al. 1998; Gill & Heyl 2007), which corresponds to $10^4 - 10^5 \text{ Gpc}^{-3} \text{ yr}^{-1}$, and implies that the magnetar production rate is a substantial fraction of the CCSNe rate.

However, the fraction of magnetars that are created with the necessary millisecond spin periods to power magnetar-driven transients is much smaller. Indeed, should all magnetars be created with such periods we should observe their enhanced energy input in the light curves of a large fraction of SNe. Instead, observations of SNe suggest that only a small fraction is consistent with the high luminosities that would be obtained via magnetar spin-down power (e.g., Rea et al. 2015, also see Nakar & Piro 2014 and Rodríguez et al. 2024). Indeed, Rea et al. (2015) suggest that extreme transients require an additional population of "super-magnetars" (millisecond magnetars), substantially rarer than the general population. These objects are estimated to form at a rate of $\leq 16 \text{ Myr}^{-1}$ in the MW – significantly rarer than the CCSNe event rate in the MW $\sim 10^4 \text{ Myr}^{-1}$ (Rozwadowska et al. 2021). This implies that $< 0.2\%$ of CCSNe events could potentially produce millisecond magnetars, i.e., $\sim 20 \text{ Myr}^{-1}$ in the MW or $< 10^2 \text{ Gpc}^{-3} \text{ yr}^{-1}$.

The challenge in obtaining millisecond magnetars in core collapse is that angular momentum conservation must enable a nascent NS with a rotation period of millisecond duration. Specifically, millisecond magnetars, rather like BH engines in GRBs require specific angular momentum (angular momentum per unit mass) of $j \gtrsim 10^{16} \text{ cm}^2 \text{ s}^{-1}$ (Levan et al. 2016). However, massive single stars spin down due to mass and angular momentum loss via stellar winds and obtaining the necessary rotation requires binary interactions (e.g., Ghodla et al. 2022), for example. While substantial uncertainties remain on how the core couples to its envelope, and in the detailed stellar evolution it is clear that only a small minority of core collapse events can create magnetars with millisecond spin periods, and that this fraction may be strongly metallicity dependent.

3. Discussion

3.1. Event Rate Conversion

Throughout this paper, we refer to literature that provides the event rates in different units. Several papers estimate event rates in the context of the Milky Way (MW) (e.g., Nelemans et al. 2001; Levan et al. 2006) while some others calculate the volumetric event rates (e.g., Abbott et al. 2023; Zhong & Dai 2020). To be able to compare the different formation scenarios and the FXT event rate, it is important to convert all the rates to the same volumetric units of $\text{Gpc}^{-3} \text{ yr}^{-1}$. We describe the method we use for this below.

To calculate the volumetric rate \mathcal{R} , we follow the form of equation 7 in Kopparapu et al. 2008 and rewrite it considering two different cases: \mathcal{R}_{SMD} and \mathcal{R}_{SFR} . First, we consider scenarios that depend on the galaxy stellar mass density (SMD) present at each epoch, rather than ongoing star formation. This is more suitable for binary merger scenarios, especially those with longer delay times between star formation and the merger. The galaxy SMD decreases with increasing redshift, reflecting the buildup of stellar mass as the universe ages. We have,

$$\mathcal{R}_{\text{SMD}} = \frac{r_{\text{MW}}}{M_{\text{MW}}} \rho^*, \quad (1)$$

where $r_{\text{MW}} [\text{yr}^{-1}]$ is the event rate in the MW, $M_{\text{MW}} \sim 10^{10} M_\odot$ (e.g., Licquia & Newman 2015) is the stellar mass of the MW, and $\rho^* [M_\odot \text{ Gpc}^{-3}]$ is the galaxy SMD (see table C.1. in Weaver et al. 2023).

Second, we consider the volumetric rate as a function of the evolution of the star formation rate (SFR) with redshift, this is relevant for formation mechanisms that are strongly linked to star formation, such as the collapse of massive stars and binary mergers with short delay times. Thus, we have

$$\mathcal{R}_{\text{SFR}} = \frac{r_{\text{MW}}}{\text{SFR}_{\text{MW}}} \text{SFR}(z), \quad (2)$$

where $\text{SFR}_{\text{MW}} \sim 2.0 \pm 0.7 M_\odot \text{ yr}^{-1}$ is the current star formation rate of the MW (e.g., Elia et al. 2022), and $\text{SFR}(z)$ is the SFR density as a function of redshift, given by Madau & Dickinson (2014):

$$\text{SFR}(z) = 0.015 \frac{(1+z)^{2.7}}{1 + [(1+z)/2.9]^{5.6}} M_\odot \text{ Mpc}^{-3} \text{ yr}^{-1}. \quad (3)$$

The $\text{SFR}(z)$ distribution peaks at $z \sim 2$, so the volumetric rate is highest at that redshift.

The BWD merger rate in the MW is $3 \times 10^{-3} \text{ yr}^{-1}$ (Nelemans et al. 2001), this can be converted to $\mathcal{R}_{\text{SFR}} \sim 10^4 \text{ Gpc}^{-3} \text{ yr}^{-1}$ and $\mathcal{R}_{\text{SMD}} \sim 10^3 - 10^4 \text{ Gpc}^{-3} \text{ yr}^{-1}$. Similarly, the rate of production of magnetars from BWD mergers is $3 \times 10^{-4} \text{ yr}^{-1}$ Levan et al. (2006), and the NSWD merger rate in the MW is $10^{-6} - 10^{-3} \text{ yr}^{-1}$ (Kim et al. 2004; Portegies Zwart & Yungelson 1999; Tauris & Sennels 2000; Davies et al. 2002); the corresponding converted volumetric rate values for each of these scenarios is listed in Table 1 (also see Figure 2). It is important to note that in our event rate conversion, we consider the stellar masses of the galaxies instead of their blue-light luminosities. Previously, the number of Milky Way Equivalent Galaxies (MWEG), n_{MWEG} , was calculated by considering the blue-light luminosity of galaxies, corrected for

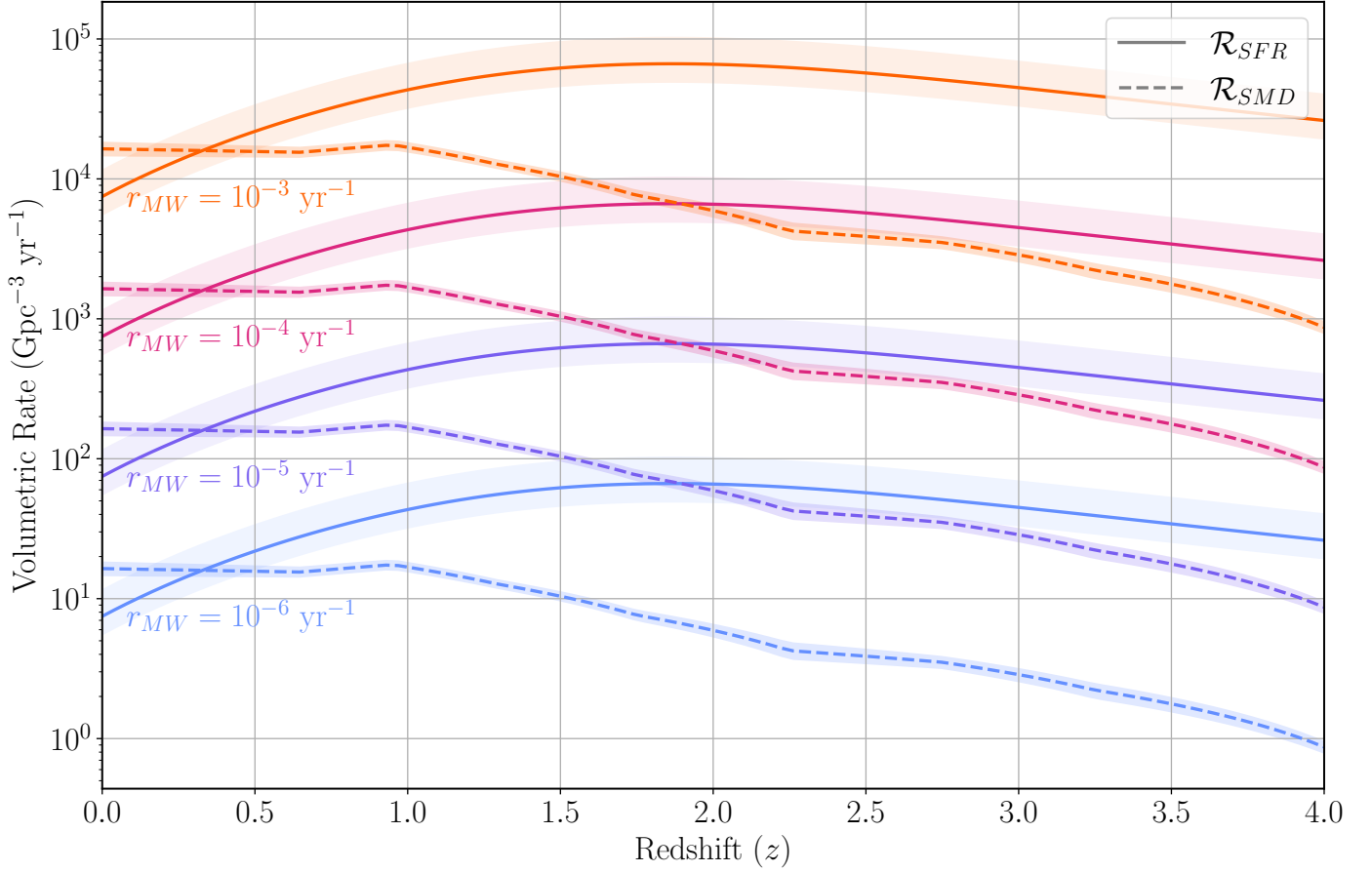


Fig. 2. Volumetric rates as a function of redshift calculated using two different methods: galaxy SMD (\mathcal{R}_{SMD} dashed lines) suitable for binary mergers with longer delay times between star formation and the merger, and SFR density (\mathcal{R}_{SFR} , solid lines) suitable for events strongly linked to star formation such as the collapse of massive stars and binary mergers with shorter delay times between star formation and the merger. The rates are computed for different MW event rates (r_{MW}) ranging from 10^{-6} to 10^{-3} yr^{-1} .

Table 1. Volumetric rates calculated using SFR density (\mathcal{R}_{SFR}) and galaxy SMD (\mathcal{R}_{SMD}) methods at different redshifts for various MW event rates $r_{\text{MW}}[\text{yr}^{-1}]$

z	$r_{\text{MW}} = 10^{-3}$	$r_{\text{MW}} = 10^{-4}$	$r_{\text{MW}} = 10^{-5}$	$r_{\text{MW}} = 10^{-6}$
$\mathcal{R}_{\text{SFR}} (\text{Gpc}^{-3} \text{ yr}^{-1})$				
$z = 0.3$	$(1.71^{+0.92}_{-0.44}) \times 10^4$	$(1.71^{+0.92}_{-0.44}) \times 10^3$	$(1.71^{+0.92}_{-0.44}) \times 10^2$	$(1.71^{+0.92}_{-0.44}) \times 10^1$
$z = 1.0$	$(4.38^{+2.36}_{-1.14}) \times 10^4$	$(4.38^{+2.36}_{-1.14}) \times 10^3$	$(4.38^{+2.36}_{-1.14}) \times 10^2$	$(4.38^{+2.36}_{-1.14}) \times 10^1$
$z = 2.0$	$(6.58^{+3.54}_{-1.70}) \times 10^4$	$(6.58^{+3.54}_{-1.70}) \times 10^3$	$(6.58^{+3.54}_{-1.70}) \times 10^2$	$(6.58^{+3.54}_{-1.70}) \times 10^1$
$z = 3.0$	$(4.42^{+2.38}_{-1.15}) \times 10^4$	$(4.42^{+2.38}_{-1.15}) \times 10^3$	$(4.42^{+2.38}_{-1.15}) \times 10^2$	$(4.42^{+2.38}_{-1.15}) \times 10^1$
$z = 4.0$	$(2.61^{+1.41}_{-0.68}) \times 10^4$	$(2.61^{+1.41}_{-0.68}) \times 10^3$	$(2.61^{+1.41}_{-0.68}) \times 10^2$	$(2.61^{+1.41}_{-0.68}) \times 10^1$
$\mathcal{R}_{\text{SMD}} (\text{Gpc}^{-3} \text{ yr}^{-1})$				
$z = 0.3$	$(1.59^{+0.15}_{-0.14}) \times 10^4$	$(1.59^{+0.15}_{-0.14}) \times 10^3$	$(1.59^{+0.15}_{-0.14}) \times 10^2$	$(1.59^{+0.15}_{-0.14}) \times 10^1$
$z = 1.0$	$(1.67^{+0.13}_{-0.12}) \times 10^4$	$(1.67^{+0.13}_{-0.12}) \times 10^3$	$(1.67^{+0.13}_{-0.12}) \times 10^2$	$(1.67^{+0.13}_{-0.12}) \times 10^1$
$z = 2.0$	$(5.80^{+0.60}_{-0.58}) \times 10^3$	$(5.80^{+0.60}_{-0.58}) \times 10^2$	$(5.80^{+0.60}_{-0.58}) \times 10^1$	$(5.80^{+0.60}_{-0.58}) \times 10^0$
$z = 3.0$	$(2.79^{+0.28}_{-0.30}) \times 10^3$	$(2.79^{+0.28}_{-0.30}) \times 10^2$	$(2.79^{+0.28}_{-0.30}) \times 10^1$	$(2.79^{+0.28}_{-0.30}) \times 10^0$
$z = 4.0$	$(8.70 \pm 0.80) \times 10^2$	$(8.70 \pm 0.80) \times 10^1$	$(8.70 \pm 0.80) \times 10^0$	$(8.70 \pm 0.80) \times 10^{-1}$

\mathcal{R}_{SFR} values are derived assuming $\text{SFR}_{\text{MW}} = 2.0 \pm 0.7 \text{ M}_{\odot} \text{ yr}^{-1}$.

\mathcal{R}_{SMD} values are calculated using ρ^* values from table C.1 in Weaver et al. 2023.

Table 2. Volumetric rate of formation of magnetars from compact object scenarios

Pathway	Event	Magnetar Formation Rate ^(a)	Millisecond Magnetar Formation Rate ^(a)
A	BWD	$< 10^3 - 10^5$ ^(b)	$< 10^4$
B	AIC of WD	$< 10^1 - 10^3$ ^(b)	< 10
C	NSWD	150 – 300	–
D	BNS	$10^1 - 10^3$	$\lesssim 8.5 \times 10^2$ ^(c)
E	Massive Stars	$10^4 - 10^5$	$< 10^2$

^(a) Rates are given in $\text{Gpc}^{-3} \text{ yr}^{-1}$;^(b) Event rate, therefore an upper limit for magnetar formation;^(c) Estimated from table 3 in Metzger (2019);

$$B_{\text{magnetar}} = B_{\text{WD}} \left(\frac{R_{\text{WD}}}{R_{\text{magnetar}}} \right)^2$$

$$P_{\text{magnetar}} = P_{\text{WD}} \left(\frac{R_{\text{magnetar}}}{R_{\text{WD}}} \right)^2, \quad (4)$$

where $R_{\text{magnetar}} = 10 \text{ km}$, and $R_{\text{WD}} = 10^4 \text{ km}$. To achieve $B_{\text{magnetar}} = 10^{14} - 10^{16} \text{ G}$ and $P_{\text{magnetar}} = 1 - 2 \text{ ms}$, we require at least one of the WD progenitors to have $B_{\text{WD}} \gtrsim 10^8 \text{ G}$ and $P_{\text{WD}} \approx 10^3 \text{ s}$. About 10% of WDs have fields in excess of 10^6 G (Kawka & Vennes 2007), with the fraction of WDs with fields $\gtrsim 10^8 \text{ G}$ considerably smaller, i.e., $\sim 2 - 4\%$ (see figure 2 in Wickramasinghe & Ferrario 2005 and figure 5 in Mohapatra & Blackman 2024). Furthermore, observations indicate that magnetic WDs exhibit a wide range of rotational periods, from minutes to years, with the most strongly magnetized WDs tending to be slower rotators (Ferrario et al. 2015). These observational constraints suggest that only a very small fraction of WDs meet the criteria necessary for millisecond magnetar formation through BWD mergers.

dust extinction and reddening (Phinney 1991), as a measure of star formation. However, blue-light luminosity may not be a perfect tracer of current SFR (e.g., Abadie et al. 2010), and instead Equation 3 provides a better estimate (Madau & Dickinson 2014). While the MWEF method using blue-light luminosity has been effective for local universe estimates, considering the SFR and SMD densities encompasses redshift evolution. The SFR density peaks at $z \sim 2$ with values ~ 10 times higher than at $z=0$, while the SMD shows a continuous increase towards $z = 0$, making this approach useful for calculating rates of events with different delay times relative to star formation.

3.2. Spin Distribution & Magnetic Field Strength Distribution Uncertainties

There are significant uncertainties in the initial spin periods and magnetic field strength distribution of newly-formed magnetars in all the formation pathways that we discuss in Section 2. In this subsection, we discuss those originating from the collapse of massive stars and BWD mergers, as these pathways exhibit the highest volumetric rates for millisecond magnetar production, thereby representing the most viable formation channels. For magnetars formed during the collapse of a massive star, several factors such as the mass of the star, metallicity (Song & Liu 2023), and magnetic field configuration (e.g., Duncan & Thompson 1992) contribute to the uncertainty in the initial spin period distribution. Some models suggest millisecond periods for dynamo-generated fields (Duncan & Thompson 1992). Jawor & Tauris (2021) uses population synthesis models to provide an upper bound, concluding that the initial spin period of magnetars must be less than 2 s. This is in agreement with observations of SN remnants around some magnetars that suggest initial spin periods $> 5 \text{ ms}$ (Vink & Kuiper 2006; Zhou, Ping et al. 2019).

In the case of BWD mergers that produce a magnetar remnant, and assuming conservation of angular momentum, we can link properties of the newly formed magnetar to those of the progenitor WDs by considering the following simplified equations (Kremer et al. 2023):

3.3. CCSNe: Surrounding Ejecta

Lamb et al. 2004 proposed that both GRBs and X-ray flashes (XRFs) stem from narrowly collimated jets produced by the collapse of massive stars, implying a population of events similar to FXTs. Early evidence supporting this idea has emerged from follow-up studies of EP FXTs (van Dalen et al. 2025; Rastinejad et al. 2025; Eyles-Ferris et al. 2025). However, some low-redshift EP FXTs do not show signs of a SN (e.g., Rayson et al., *in prep*) which makes it unlikely that all FXTs are the result of collapsars. While the collapse of massive stars is indeed a potential formation channel for FXT-producing millisecond magnetars, this scenario faces significant observational challenges, which we discuss in detail below.

CCSNe typically eject $1-15 M_{\odot}$ of material, expanding at velocities of $\sim 10^4 \text{ km s}^{-1}$ (Haynie & Piro 2023; Zha et al. 2024), resulting in an optically thick envelope that remains opaque to X-rays for weeks to months, thus preventing the observation of the characteristic X-ray emission of FXTs. As the SN ejecta expands and becomes less dense, the X-rays are absorbed by the surrounding ejecta and thermalized into optical radiation (Metzger et al. 2015). This thermalization mechanism is well-established in the context of superluminous supernovae (SLSNe), for which millisecond magnetars are considered to be the central engines powering them by converting the initial X-ray emission into optical radiation. This connection between millisecond magnetars and SLSNe is supported by observations such as SLSNe SCP06F6 (Levan et al. 2013), which showed an X-ray outburst with a peak luminosity of $L_X \sim 10^{45} \text{ erg s}^{-1}$ and a duration of $\lesssim 10 \text{ ks}$, similar to the expected FXT luminosities and durations.

The general yet uncertain idea is that the conservation of angular momentum during the collapse of the massive star causes the core to spin faster, which creates a jet that emerges from the collapsing star. It is collimated and accelerated by the magnetic field, and it propagates through the surrounding SN ejecta (Levan et al. 2016; and references therein). This could provide a pathway for the X-ray

emission to escape the dense SN ejecta, while simultaneously interacting with the surrounding medium to produce optical emission (Margalit et al. 2018). For example, recent observations of EP240414a demonstrate that jet formation within a dense stellar envelope can produce X-ray outbursts reaching luminosities of $\sim 10^{48}$ erg s $^{-1}$ (van Dalen et al. 2024). However, previous studies have raised important challenges to the rapid-rotation scenario for magnetar formation in CCSNe. Simulations suggest that magnetic fields can be amplified to magnetar field strengths even in slowly-rotating progenitors through small-scale dynamo action (Müller & Varma 2020). Moreover, observational studies of SN remnants containing magnetars show no evidence of enhanced explosion energies that would be expected from rapidly rotating NSs, or millisecond magnetars. These remnants show explosion energies consistent with $\sim 10^{51}$ erg, suggested initial spin periods > 5 ms (Vink 2008). While fallback accretion could potentially mask some signatures of rapid rotation by modifying the explosion energetics and remnant properties (e.g., Metzger et al. 2018; Wei et al. 2021), the combined theoretical and observational constraints suggest that extreme rapid rotation may not be necessary for magnetar formation (Torres-Forné et al. 2016).

Another key factor to consider is the metallicity of the star, which plays a critical role in both the formation of the central engine and the jet collimation (if it is indeed produced). Lower metallicity stars tend to retain more of their initial angular momentum due to reduced mass loss through stellar winds (Georgy et al. 2011) which leads to rapid rotation, and are more likely to collapse into millisecond magnetars (Levan et al. 2016) (see their figure 7). Consequently, the formation efficiency of millisecond magnetars may exhibit a metallicity dependence, with potentially higher rates occurring in low-metallicity stars (Song & Liu 2023). Further, in low-metallicity stars, the jet is probably more narrowly collimated (Mizuta & Aloy 2009). Hence, the massive stars that collapse to produce millisecond magnetars tend to generate highly collimated jets reducing the likelihood of detecting FXTs from these events, and may also explain the non-detection of gamma rays in some FXTs.

3.4. Implications for the Origin of FXTs

To consider the implications for the origin of FXTs, it is important to first note that not all FXTs are alike and they potentially arise from different origins, for example, XRT 110621 is suggested to be from a SN SBO origin (Alp & Larsson 2020; Eappachen et al. 2024), XRT 100831 is suggested to be a WD-IMBH TDE (Quirola-Vásquez et al. 2022, 2024; Inkenhaag et al. 2024) and XRT 030206 possibly has a BNS origin (Alp & Larsson 2020; Eappachen et al. 2024); this implies that only a fraction of all FXTs can be linked to a millisecond magnetar origin.

Some detected FXTs were found to be associated with GRBs, as confirmed by contemporaneous GRB detections, for example, EP240315a (Levan et al. 2024b) and EP240219a (Yin et al. 2024). Population synthesis studies of Galactic magnetars reveal that ≤ 16 Myr $^{-1}$ (millisecond) magnetars could have formed via GRB-like events (Rea et al. 2015). Using the method described in Section 3.1, this corresponds to, and provides us with an upper limit of $\mathcal{R}_{\text{SFR}} \approx 10^2 - 10^3$ Gpc $^{-3}$ yr $^{-1}$ and $\mathcal{R}_{\text{SMD}} \approx$

$10^1 - 10^2$ Gpc $^{-3}$ yr $^{-1}$. Given that the detected FXT rate is $\approx 10^3 - 10^4$ Gpc $^{-3}$ yr $^{-1}$, this constraint suggests that millisecond magnetars can account for at most 10% of the total detected FXT population.

Further, we compare the Galactic magnetar rate of ≤ 16 Myr $^{-1}$ to the rate of formation of millisecond magnetars from BWD mergers in the MW, i.e., ~ 300 Myr $^{-1}$ (Levan et al. 2006), and the BNS merger rate in the MW, ~ 30 Myr $^{-1}$ (Sgalletta et al. 2023). The lower rate of Galactic magnetars implies that most BWD and BNS merger products must either collapse promptly to form BHs or form unstable magnetars that quickly collapse. Finally, the ~ 20 Myr $^{-1}$ rate from the collapse of massive stars (Section 2.5) aligns with the Galactic magnetar rate, positioning this channel as a plausible, although rare, contributor to the FXT population.

3.5. Implications for the Origin of Other Transients

Millisecond magnetars have been proposed as the central engine for several classes of energetic transients beyond FXTs (e.g., Metzger et al. 2015). These include superluminous supernovae (SLSNe) (e.g., Nicholl et al. 2015; Vurm & Metzger 2021; Gottlieb & Metzger 2024), long and short gamma-ray bursts (LGRBs and SGRBs) (e.g., Lü et al. 2015; Levan et al. 2016; Sarin et al. 2020), fast radio bursts (FRBs) (e.g., Metzger et al. 2017; Nicholl et al. 2017; Safarzadeh et al. 2020), and fast blue optical transients (FBOTs) (e.g., Yao et al. 2022; Li et al. 2024). The rapid rotation and strong magnetic fields of millisecond magnetars can power these events through different mechanisms, e.g., the spin-down energy injection can produce the extraordinary luminosity of SLSNe, or drive the relativistic outflows in GRBs, and generate coherent radio emission in FRBs. Each transient class occupies a distinct region in the parameter space of magnetic field strength, initial spin period, and ejecta mass, suggesting different formation channels. While our derived constraints on the millisecond magnetar formation rates could have important implications for the rates of these transient populations, a detailed comparison of their event rates and the required magnetar formation efficiency for each class extends beyond the scope of this work.

4. Conclusion

FXTs are short X-ray flashes with durations of a few minutes to hours, that have been detected by telescopes such as *Chandra*, *XMM-Newton*, and *Swift-XRT* at a rate of $10^3 - 10^4$ Gpc $^{-3}$ yr $^{-1}$ over the last two decades. With the launch of *Einstein Probe (EP)* in early 2024, there have been many more FXT detections even during its commissioning phase (that ended in July 2024) and since the start of nominal operations. While several theories have been proposed, the origin of FXTs is not yet understood. One model invokes the spin-down of a highly magnetic, millisecond spin NS, or a millisecond magnetar, produced as a post-merger remnant of a BNS merger. In this paper, we consider all possible formation pathways for millisecond magnetars that can produce an FXT, such as the AIC of

² Quirola-Vásquez et al. (2022, 2023) calculate the FXT event rate up to $z \sim 2$, whereas we are extrapolating \mathcal{R}_{SFR} and \mathcal{R}_{SMD} to $z \sim 4$, however this does not alter the conclusions we present here.

massive WDs, BWD, NSWd and BNS mergers, and the collapse of massive stars, and compare it to the FXT rate. We find that the highest rate of formation of (millisecond) magnetars is from massive stars, followed by BWD mergers and BNS mergers. Several key factors limit the viability of millisecond magnetars as FXT progenitors such as the uncertainties in the spin and magnetic field distributions of magnetars in all the scenarios we have discussed, and the presence of dense surrounding ejecta preventing the detection of X-rays on timescales compatible with the duration of FXTs along with other observational constraints, in the case of CCSNe. The requirement for both rapid rotation on \sim millisecond timescales, and strong magnetic field strengths of $10^{14} - 10^{15}$ G, significantly reduces the fraction of events that could result in the formation of millisecond magnetars, and in several cases, the exact fraction is difficult to precisely constrain. With *EP* now detecting several FXTs, the diversity in the FXT properties suggests that FXTs arise from different origins, and millisecond magnetars can account for at most 10% of the entire FXT population. Future observations, particularly with rapid multi-wavelength follow-up, and the identification of the host galaxies of FXTs, will be crucial for determining the relative contributions of different progenitor scenarios.

Acknowledgements. SB would like to thank Ilya Mandel for his helpful inputs during discussions related to this project. SB acknowledges studentship support from the Dutch Research Council (NWO) under the project number 680.92.18.02. PGJ is supported by the European Union (ERC, StarStruck, 101095973). Views and opinions expressed are however those of the author(s) only and do not necessarily reflect those of the European Union or the European Research Council. Neither the European Union nor the granting authority can be held responsible for them. This work made use of Python packages NUMPY (Harris et al. 2020), SCIPY (Virtanen et al. 2020), and MATPLOTLIB (Hunter 2007). This work made use of ASTROPY: a community-developed core Python package and an ecosystem of tools and resources for astronomy (Astropy Collaboration et al. 2013, 2018, 2022). We thank the referee for the insightful comments on this manuscript.

References

- Abadie, J., Abbott, B. P., Abbott, R., et al. 2010, *Classical and Quantum Gravity*, 27, 173001
- Abbott, R., Abbott, T. D., Acernese, F., et al. 2023, *Phys. Rev. X*, 13, 011048
- Acharya, S. K., Beniamini, P., & Hotokezaka, K. 2025, *A&A*, 693, A108
- Alp, D. & Larsson, J. 2020, *ApJ*, 896, 39
- Antoniadis, J., Freire, P. C. C., Wex, N., et al. 2013, *Science*, 340, 448
- Astropy Collaboration, Price-Whelan, A. M., Lim, P. L., et al. 2022, *ApJ*, 935, 167
- Astropy Collaboration, Price-Whelan, A. M., Sipőcz, B. M., et al. 2018, *AJ*, 156, 123
- Astropy Collaboration, Robitaille, T. P., Tollerud, E. J., et al. 2013, *A&A*, 558, A33
- Bauer, F. E., Treister, E., Schawinski, K., et al. 2017, *MNRAS*, 467, 4841
- Bauswein, A., Baumgarte, T. W., & Janka, H. T. 2013, *Phys. Rev. Lett.*, 111, 131101
- Beniamini, P., Hotokezaka, K., van der Horst, A., & Kouveliotou, C. 2019, *Monthly Notices of the Royal Astronomical Society*, 487, 1426–1438
- Beniamini, P. & Lu, W. 2021, *ApJ*, 920, 109
- Bruni, G., Rhodes, L., Piro, L., et al. 2024, *GRB Coordinates Network*, 35980, 1
- Carotenuto, F., Bright, J., Jonker, P. G., Fender, R., & Rhodes, L. 2024, *GRB Coordinates Network*, 35961, 1
- Chandrasekhar, S. 1931, *ApJ*, 74, 81
- Cumming, A., Arras, P., & Zweibel, E. 2004, *ApJ*, 609, 999
- Dai, L., McKinney, J. C., Roth, N., Ramirez-Ruiz, E., & Miller, M. C. 2018, *ApJ*, 859, L20
- Dan, M., Rosswog, S., Brüggen, M., & Podsiadlowski, P. 2013, *Monthly Notices of the Royal Astronomical Society*, 438, 14
- Davies, M. B., Ritter, H., & King, A. 2002, *MNRAS*, 335, 369
- D’Elia, V., Campana, S., D’Ai, A., et al. 2018, *A&A*, 619, A66
- Demorest, P. B., Pennucci, T., Ransom, S. M., Roberts, M. S. E., & Hessels, J. W. T. 2010, *Nature*, 467, 1081
- Duncan, R. C. & Thompson, C. 1992, *ApJ*, 392, L9
- Eappachen, D., Jonker, P. G., Fraser, M., et al. 2022, *MNRAS*, 514, 302
- Eappachen, D., Jonker, P. G., Levan, A. J., et al. 2023, *ApJ*, 948, 91
- Eappachen, D., Jonker, P. G., Quirola-Vásquez, J., et al. 2024, *MNRAS*, 527, 11823
- Eldridge, J. J., Stanway, E. R., & Tang, P. N. 2019, *MNRAS*, 482, 870
- Elia, D., Molinari, S., Schisano, E., et al. 2022, *The Astrophysical Journal*, 941, 162
- Eyles-Ferris, R. A. J., Jonker, P. G., Levan, A. J., et al. 2025, *arXiv e-prints*, arXiv:2504.08886
- Ferrario, L., de Martino, D., & Gänsicke, B. T. 2015, *Space Sci. Rev.*, 191, 111
- Fong, W., Berger, E., Margutti, R., & Zauderer, B. A. 2015, *ApJ*, 815, 102
- Georgy, C., Meynet, G., & Maeder, A. 2011, *A&A*, 527, A52
- Ghodla, S., Eldridge, J. J., Stanway, E. R., & Stevance, H. F. 2022, *Monthly Notices of the Royal Astronomical Society*, 518, 860–877
- Giacomazzo, B., Zrake, J., Duffell, P. C., MacFadyen, A. I., & Perna, R. 2015, *ApJ*, 809, 39
- Gill, R. & Heyl, J. 2007, *MNRAS*, 381, 52
- Gillanders, J. H., Rhodes, L., Srivastav, S., et al. 2024, *ApJ*, 969, L14
- Glennie, A., Jonker, P. G., Fender, R. P., Nagayama, T., & Pretorius, M. L. 2015, *MNRAS*, 450, 3765
- Gottlieb, O. & Metzger, B. D. 2024, *ApJ*, 974, L9
- Granot, J., Guetta, D., & Gill, R. 2017, *ApJ*, 850, L24
- Hachisu, I., Kato, M., & Nomoto, K. 1996, *ApJ*, 470, L97
- Harris, C. R., Millman, K. J., van der Walt, S. J., et al. 2020, *Nature*, 585, 357
- Haynie, A. & Piro, A. L. 2023, *The Astrophysical Journal*, 956, 98
- Hjellming, M. S. & Webbink, R. F. 1987, *ApJ*, 318, 794
- Holberg, J. B. 2009, in *Journal of Physics Conference Series*, Vol. 172, *Journal of Physics Conference Series* (IOP), 012022
- Horesh, A., Hotokezaka, K., Piran, T., Nakar, E., & Hancock, P. 2016, *ApJ*, 819, L22
- Hotokezaka, K., Kiuchi, K., Kyutoku, K., et al. 2013, *Phys. Rev. D*, 87, 024001
- Hotokezaka, K., Kyutoku, K., Okawa, H., Shibata, M., & Kiuchi, K. 2011, *Phys. Rev. D*, 83, 124008
- Hunter, J. D. 2007, *Computing in Science & Engineering*, 9, 90
- Ide, S., Hayashida, K., Noda, H., et al. 2020, *PASJ*, 72, 40
- Inkenhaag, A., Jonker, P. G., Levan, A. J., et al. 2024, *Redshifts of candidate host galaxies of four fast X-ray transients using VLT/MUSE*
- Irwin, J. A., Maksym, W. P., Sivakoff, G. R., et al. 2016, *Nature*, 538, 356
- Jawor, J. A. & Tauris, T. M. 2021, *Monthly Notices of the Royal Astronomical Society*, 509, 634–657
- Jones, S., Röpke, F. K., Fryer, C., et al. 2019, *A&A*, 622, A74
- Jones, S., Röpke, F. K., Pakmor, R., et al. 2016, *A&A*, 593, A72
- Jonker, P. G., Glennie, A., Heida, M., et al. 2013, *ApJ*, 779, 14
- Kashyap, R., Haque, T., Lorén-Aguilar, P., García-Berro, E., & Fisher, R. 2018, *The Astrophysical Journal*, 869, 140
- Kawka, A. & Vennes, S. 2007, in *UV Astronomy: Stars from Birth to Death*, ed. A. I. Gómez de Castro & M. A. Barstow, 237–242
- Kim, C., Kalogera, V., Lorimer, D. R., & White, T. 2004, *ApJ*, 616, 1109
- King, A. R., Pringle, J. E., & Wickramasinghe, D. T. 2001, *MNRAS*, 320, L45
- Konar, S. & Bhattacharya, D. 1997, *MNRAS*, 284, 311
- Kopparapu, R. K., Hanna, C., Kalogera, V., et al. 2008, *ApJ*, 675, 1459
- Kouveliotou, C., Dieters, S., Strohmayer, T., et al. 1998, *Nature*, 393, 235
- Kremer, K., Li, D., Lu, W., Piro, A. L., & Zhang, B. 2023, *ApJ*, 944, 6
- Külebi, B., Ekşi, K. Y., Lorén-Aguilar, P., Isern, J., & García-Berro, E. 2013, *Monthly Notices of the Royal Astronomical Society*, 431, 2778–2788

- Lamb, D., Donaghy, T., & Graziani, C. 2004, *New Astronomy Reviews*, 48, 459, 2nd VERITAS Symposium on the Astrophysics of Extragalactic Sources
- Leung, J. K., Ricci, R., Dobie, D., & Troja, E. 2024, *GRB Coordinates Network*, 35968, 1
- Levan, A., Crowther, P., de Grijs, R., et al. 2016, *Space Sci. Rev.*, 202, 33
- Levan, A. J., Jonker, P. G., Saccardi, A., et al. 2024a, arXiv e-prints, arXiv:2404.16350
- Levan, A. J., Jonker, P. G., Saccardi, A., et al. 2024b, arXiv e-prints, arXiv:2404.16350
- Levan, A. J., Read, A. M., Metzger, B. D., Wheatley, P. J., & Tanvir, N. R. 2013, *The Astrophysical Journal*, 771, 136
- Levan, A. J., Wynn, G. A., Chapman, R., et al. 2006, *Monthly Notices of the Royal Astronomical Society: Letters*, 368, L1
- Li, L., Zhong, S.-Q., Xiao, D., et al. 2024, *ApJ*, 963, L13
- Li, X. D. & van den Heuvel, E. P. J. 1997, *A&A*, 322, L9
- Licquia, T. C. & Newman, J. A. 2015, *The Astrophysical Journal*, 806, 96
- Lin, D., Irwin, J. A., & Berger, E. 2021, *The Astronomer's Telegram*, 14599, 1
- Lin, D., Irwin, J. A., Berger, E., & Nguyen, R. 2022, *ApJ*, 927, 211
- Lin, D., Strader, J., Carrasco, E. R., et al. 2018, *Nature Astronomy*, 2, 656
- Lin, D., Strader, J., Romanowsky, A. J., et al. 2020, *ApJ*, 892, L25
- Liu, D. & Wang, B. 2020, *MNRAS*, 494, 3422
- Liu, Y., Sun, H., Xu, D., et al. 2024, *Soft X-ray prompt emission from a high-redshift gamma-ray burst EP240315a*
- Lorimer, D. R. 2005, *Living Reviews in Relativity*, 8, 7
- Lü, H.-J., Zhang, B., Lei, W.-H., Li, Y., & Lasky, P. D. 2015, *ApJ*, 805, 89
- Lyman, J. D., Levan, A. J., Wiersema, K., et al. 2022, *ApJ*, 926, 121
- MacLeod, M., Goldstein, J., Ramirez-Ruiz, E., Guillochon, J., & Samising, J. 2014, *ApJ*, 794, 9
- Madau, P. & Dickinson, M. 2014, *ARA&A*, 52, 415
- Maguire, K., Eracleous, M., Jonker, P. G., MacLeod, M., & Rosswog, S. 2020, *Space Sci. Rev.*, 216, 39
- Mandel, I. & Broekgaarden, F. S. 2022, *Living Reviews in Relativity*, 25
- Margalit, B., Jermyn, A. S., Metzger, B. D., Roberts, L. F., & Quataert, E. 2022, *ApJ*, 939, 51
- Margalit, B. & Metzger, B. D. 2016, *MNRAS*, 461, 1154
- Margalit, B. & Metzger, B. D. 2017, *ApJ*, 850, L19
- Margalit, B., Metzger, B. D., Thompson, T. A., Nicholl, M., & Sukhbold, T. 2018, *Monthly Notices of the Royal Astronomical Society*, 475, 2659–2674
- Mazzali, P. A., Valenti, S., Della Valle, M., et al. 2008, *Science*, 321, 1185
- Metzger, B. D. 2012, *MNRAS*, 419, 827
- Metzger, B. D. 2019, *Living Reviews in Relativity*, 23, 1
- Metzger, B. D., Beniamini, P., & Giannios, D. 2018, *The Astrophysical Journal*, 857, 95
- Metzger, B. D., Berger, E., & Margalit, B. 2017, *ApJ*, 841, 14
- Metzger, B. D., Margalit, B., Kasen, D., & Quataert, E. 2015, *MNRAS*, 454, 3311
- Miyaji, S., Nomoto, K., Yokoi, K., & Sugimoto, D. 1980, *PASJ*, 32, 303
- Mizuta, A. & Aloy, M. A. 2009, *The Astrophysical Journal*, 699, 1261
- Modjaz, M., Li, W., Butler, N., et al. 2009, *ApJ*, 702, 226
- Mohapatra, A. & Blackman, E. G. 2024, arXiv e-prints, arXiv:2412.05400
- Müller, B. & Varma, V. 2020, *MNRAS*, 498, L109
- Nakar, E. 2015, *ApJ*, 807, 172
- Nakar, E. & Piro, A. L. 2014, *ApJ*, 788, 193
- Nakar, E. & Sari, R. 2010, *ApJ*, 725, 904
- Napiwotzki, R. 2009, in *Journal of Physics Conference Series*, Vol. 172, *Journal of Physics Conference Series (IOP)*, 012004
- Nelemans, G., Yungelson, L. R., Portegies Zwart, S. F., & Verbunt, F. 2001, *A&A*, 365, 491
- Nicholl, M., Smartt, S. J., Jerkstrand, A., et al. 2015, *MNRAS*, 452, 3869
- Nicholl, M., Williams, P. K. G., Berger, E., et al. 2017, *The Astrophysical Journal*, 843, 84
- Novara, G., Esposito, P., Tiengo, A., et al. 2020, *ApJ*, 898, 37
- Olausen, S. A. & Kaspi, V. M. 2014, *ApJS*, 212, 6
- Pan, X., Liu, M. J., Liu, Y., et al. 2024a, *The Astronomer's Telegram*, 16564, 1
- Pan, X., Lv, Z. Z., Fu, Y. C., et al. 2024b, *GRB Coordinates Network*, 36757, 1
- Paschalidis, V., Etienne, Z., Liu, Y. T., & Shapiro, S. L. 2011, *Phys. Rev. D*, 83, 064002
- Pastor-Marazuela, I., Webb, N. A., Wojtowicz, D. T., & van Leeuwen, J. 2020, *A&A*, 640, A124
- Perets, H. B., Zenati, Y., Toonen, S., & Bobrick, A. 2019, arXiv e-prints, arXiv:1910.07532
- Peters, P. C. 1964, *Physical Review*, 136, 1224
- Phinney, E. S. 1991, *ApJ*, 380, L17
- Piro, A. L. & Kollmeier, J. A. 2016, *The Astrophysical Journal*, 826, 97
- Portegies Zwart, S. F. & Yungelson, L. R. 1999, *MNRAS*, 309, 26
- Price, D. J. & Rosswog, S. 2006, *Science*, 312, 719
- Quirola-Vásquez, J., Bauer, F. E., Jonker, P. G., et al. 2024, arXiv e-prints, arXiv:2401.01415
- Quirola-Vásquez, J., Bauer, F. E., Jonker, P. G., et al. 2023, *A&A*, 675, A44
- Quirola-Vásquez, J., Bauer, F. E., Jonker, P. G., et al. 2022, *A&A*, 663, A168
- Quirola-Vásquez, J., Bauer, F. E., Jonker, P. G., et al. 2025, *A&A*, 695, A279
- Ramirez-Ruiz, E., Celotti, A., & Rees, M. J. 2002, *MNRAS*, 337, 1349
- Rastinejad, J. C., Levan, A. J., Jonker, P. G., et al. 2025, arXiv e-prints, arXiv:2504.08889
- Rea, N., Gullón, M., Pons, J. A., et al. 2015, *The Astrophysical Journal*, 813, 92
- Ricci, R., Troja, E., Bruni, G., et al. 2021, *MNRAS*, 500, 1708
- Rodríguez, Ó., Nakar, E., & Maoz, D. 2024, *Nature*, 628, 733
- Romani, R. W., Kandel, D., Filippenko, A. V., Brink, T. G., & Zheng, W. 2022, *ApJ*, 934, L17
- Rozwadowska, K., Vissani, F., & Cappellaro, E. 2021, *New Astronomy*, 83, 101498
- Saccardi, A., Levan, A. J., Zhu, Z., et al. 2024, *GRB Coordinates Network*, 35936, 1
- Safarzadeh, M., Prochaska, J. X., Heintz, K. E., & Fong, W.-f. 2020, *ApJ*, 905, L30
- Sarin, N., Lasky, P. D., & Ashton, G. 2020, *MNRAS*, 499, 5986
- Saxton, R., Komossa, S., Auchettl, K., & Jonker, P. G. 2021, *Correction to: X-Ray Properties of TDEs*, *Space Science Reviews*, Volume 217, Issue 1, article id.18
- Schroeder, G., Margalit, B., Fong, W.-f., et al. 2020, *ApJ*, 902, 82
- Schwab, J., Quataert, E., & Kasen, D. 2016, *MNRAS*, 463, 3461
- Sgalletta, C., Iorio, G., Mapelli, M., et al. 2023, *Binary neutron star populations in the Milky Way*
- Shao, D.-S., Tang, S.-P., Sheng, X., et al. 2020, *Physical Review D*, 101
- Shen, K. J., Bildsten, L., Kasen, D., & Quataert, E. 2012, *ApJ*, 748, 35
- Shibata, M., Fujibayashi, S., Hotokezaka, K., et al. 2017, *Phys. Rev. D*, 96, 123012
- Shibata, M. & Taniguchi, K. 2006, *Phys. Rev. D*, 73, 064027
- Shibata, M. & Uryū, K. 2000, *Phys. Rev. D*, 61, 064001
- Siegel, D. M. & Cioffi, R. 2016, *ApJ*, 819, 14
- Siegel, D. M. & Cioffi, R. 2016, *The Astrophysical Journal*, 819, 15
- Sigurdsson, S. & Rees, M. J. 1997, *MNRAS*, 284, 318
- Soderberg, A. M., Berger, E., Page, K. L., et al. 2008, *Nature*, 454, 246
- Song, C.-Y. & Liu, T. 2023, *The Astrophysical Journal*, 952, 156
- Srivastav, S., Smartt, S. J., Fulton, M. D., et al. 2024, *GRB Coordinates Network*, 35932, 1
- Sun, H., Chen, W., Zhou, H., et al. 2024, *GRB Coordinates Network*, 36690, 1
- Sun, H., Li, Y., Zhang, B.-B., et al. 2019, *ApJ*, 886, 129
- Sun, H., Zhang, B., & Gao, H. 2017, in *The X-ray Universe 2017*, ed. J.-U. Ness & S. Migliari, 216
- Tauris, T. M., Sanyal, D., Yoon, S. C., & Langer, N. 2013, *A&A*, 558, A39
- Tauris, T. M. & Sennels, T. 2000, *A&A*, 355, 236
- Tendulkar, S. P., Cameron, P. B., & Kulkarni, S. R. 2012, *ApJ*, 761, 76
- Thompson, T. A., Kistler, M. D., & Stanek, K. Z. 2009, arXiv e-prints, arXiv:0912.0009
- Toonen, S., Perets, H. B., Igoshev, A. P., Michaely, E., & Zenati, Y. 2018, *A&A*, 619, A53
- Torres-Forné, A., Cerdá-Durán, P., Pons, J. A., & Font, J. A. 2016, *MNRAS*, 456, 3813
- Urpin, V., Konenkov, D., & Urpin, V. 1997, *MNRAS*, 292, 167
- van Dalen, J. N. D., Levan, A. J., Jonker, P. G., et al. 2025, *ApJ*, 982, L47

- van Dalen, J. N. D., Levan, A. J., Jonker, P. G., et al. 2024, The Einstein Probe transient EP240414a: Linking Fast X-ray Transients, Gamma-ray Bursts and Luminous Fast Blue Optical Transients
- van den Heuvel, E. P. J. & Bonsema, P. T. J. 1984, *A&A*, 139, L16
- Vink, J. 2008, *Advances in Space Research*, 41, 503
- Vink, J. & Kuiper, L. 2006, *MNRAS*, 370, L14
- Virtanen, P., Gommers, R., Oliphant, T. E., et al. 2020, *Nature Methods*, 17, 261
- Vurm, I. & Metzger, B. D. 2021, *ApJ*, 917, 77
- Wang, B. 2018, *Research in Astronomy and Astrophysics*, 18, 049
- Wang, B., Justham, S., & Han, Z. 2013, *A&A*, 559, A94
- Wang, B., Meng, X., Chen, X., & Han, Z. 2009, *MNRAS*, 395, 847
- Wang, H., Beniamini, P., & Giannios, D. 2023, Constraining the long-living supramassive neutron stars by magnetar boosted kilonovae
- Waxman, E. & Katz, B. 2017, in *Handbook of Supernovae*, ed. A. W. Alsabti & P. Murdin, 967
- Weaver, J. R., Davidzon, I., Toft, S., et al. 2023, *A&A*, 677, A184
- Wei, Y.-F., Liu, T., & Xue, L. 2021, *Monthly Notices of the Royal Astronomical Society*, 507, 431–442
- Wickramasinghe, D. T. & Ferrario, L. 2005, *Monthly Notices of the Royal Astronomical Society*, 356, 1576
- Wilms, J., Kreykenbohm, I., Weber, P., et al. 2020, *The Astronomer's Telegram*, 13416, 1
- Wu, C., Xiong, H., Han, Z., & Wang, B. 2023, *Monthly Notices of the Royal Astronomical Society*, 525, 6295
- Wu, C.-Y., Liu, D.-D., Zhou, W.-H., & Wang, B. 2016, *Research in Astronomy and Astrophysics*, 16, 160
- Wu(NAOC, Q. Y., CAS), Shui, Q. C., et al. 2024, *GRB Coordinates Network*, 36766, 1
- Xue, Y. Q., Zheng, X. C., Li, Y., et al. 2019, *Nature*, 568, 198
- Yao, Y., Ho, A. Y. Q., Medvedev, P., et al. 2022, *ApJ*, 934, 104
- Yin, Y.-H. I., Zhang, B.-B., Yang, J., et al. 2024, *ApJ*, 975, L27
- Yuan, W., Zhang, C., Chen, Y., & Ling, Z. 2022, *The Einstein Probe Mission* (Springer Nature Singapore), 1–30
- Yuan, W., Zhang, C., Feng, H., et al. 2015, *Einstein Probe - a small mission to monitor and explore the dynamic X-ray Universe*
- Yungelson, L. & Livio, M. 1998, *ApJ*, 497, 168
- Zha, S., Müller, B., & Powell, J. 2024, *The Astrophysical Journal*, 969, 141
- Zhang, B. 2013, *ApJ*, 763, L22
- Zhang, B. B., Zhang, B., Sun, H., et al. 2018, *Nature Communications*, 9, 447
- Zhang, W., Woosley, S. E., & Heger, A. 2004, *ApJ*, 608, 365
- Zhang, W. J., Mao, X., Zhang, W. D., et al. 2024, *GRB Coordinates Network*, 35931, 1
- Zheng, X. C., Xue, Y. Q., Brandt, W. N., et al. 2017, *ApJ*, 849, 127
- Zhong, S.-Q. & Dai, Z.-G. 2020, *The Astrophysical Journal*, 893, 9
- Zhou, H., Chen, W., Sun, H., et al. 2024, *GRB Coordinates Network*, 36691, 1
- Zhou, Ping, Vink, Jacco, Safi-Harb, Samar, & Miceli, Marco. 2019, *A&A*, 629, A51
- Zrake, J. & MacFadyen, A. I. 2013, *ApJ*, 769, L29